The Diameter Factor of Aligned Electrospinning Membranes Facilitates Cutaneous Wound Healing by Promoting Epithelialization

Chenbing Wang[1]; Chenyu Chu[1]; Xiwen Zhao[1]; Chen Hu[1]; Li Liu[3], Jidong Li[2], Yili Qu[1], Yi Man[1*]

1. *Department of Oral Implantology & National Clinical Research Center for Oral Diseases & State Key Laboratory of Oral Diseases, West China Hospital of Stomatology, Sichuan University, Chengdu, China*
2. *Research Center for Nano-Biomaterials, Analytical and Testing Center, Sichuan University, Chengdu 610064, China.*
3. *State Key Laboratory of Biotherapy, West China Hospital, Sichuan University, Collaborative Innovation Center for Biotherapy, Chengdu, Sichuan 610041, China*

[*] Corresponding to Professor. Chair. **Yi Man**, E-mail: manyi780203@126.com

Corresponding author:

Yi Man, DDS, PhD

Professor and Chair

Department of Oral Implantology

State Key Laboratory of Oral Diseases, West China Hospital of Stomatology, Sichuan University, 14#, 3rd section, Renmin South Road

Chengdu 610041, China

Tel: 0086-28-85503571

Fax: 0086-28-85483678

E-mail: manyi780203@126.com

Abstract：The re-epithelialization with appendages is a major challenge to skin injury. Given that topographical factors initially modulate cell activities, the design of biomaterials with the topography (such as pattern and diameter) offers a promising strategy for achieving optimal skin wound healing. Herein, we prepare an aligned fish collagen reinforced poly (lactide-co-glycolide) electrospinning membrane (FC/PLGA) with different fiber diameters including 319±100nm (A300), 687±138nm (A600) and 1048±130nm (A1000) for promoting the re-epithelialization with appendages. The A300 significantly enhanced the mechanical strength and hydrophilicity, accelerated the degradation rate, and improved the cytocompatibility (proliferation and spreading) of the FC/PLGA membrane. In particular, the A300 facilitated skin wound healing (epithelization and vascularization) with the regeneration of hair follicles (HFs). The transcriptome revealed the underlying molecular mechanism that the A300 could promote macrophages transformation to reparative phenotypes (M2), subsequently exerting anti-inflammation and promoting epidermal cell migration via secreting IL10, TGFβ and MMP12. All the results indicate the A300 to be a potential candidate for guided tissue regeneration applications.

Key words: Electrospinning; Diameter; Wound Healing; Epithelialization; MMP12

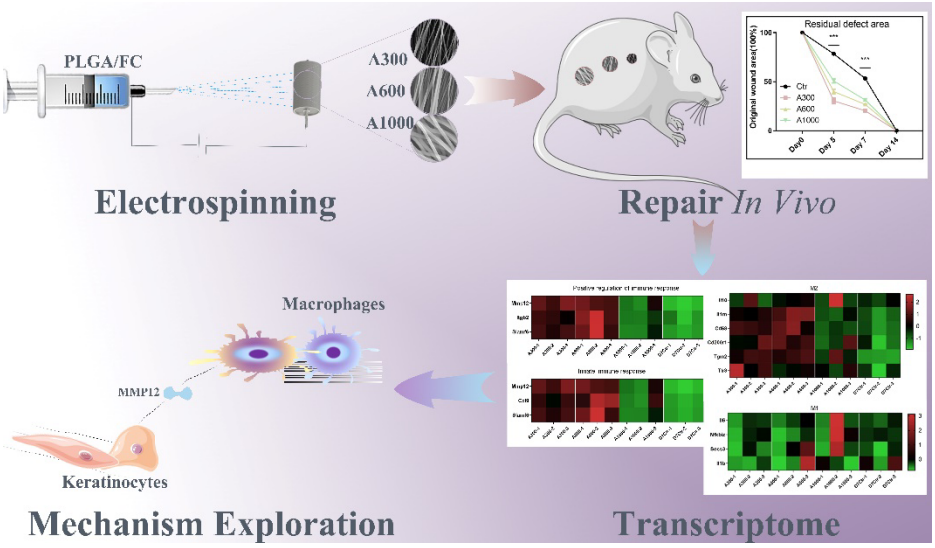

1.Introduction

Skin, as a superficial organ in contact with the surrounding environment, constitutes a first important guard-line against external hazards [1]. The inability to re-epithelialize wounded skin can contribute to dewatering, inflammation or even mortality [2,3]. Therefore, it is very important to close the wound quickly to restore the barrier function essential for survival of the organism. Regrettably, current strategies are not satisfactory in managing large and/or chronic wounds, since they are dependent on both slow and passive healing processes [4]. Promoting skin healing with the regeneration of skin appendages such as hair follicles (HFs) has not authentically been realized [5]. Consequently, there is a growing need for exploring advanced grafts to achieve ideal re-epithelialization with appendages [6-8]. Due to the characteristic of imitating the topography and functions of extracellular matrix (ECM) [9,10], providing moist environment, allowing gas exchange and avoiding bacteria infiltration[11], the electrospinning membrane is an ideal alternative for skin wound healing [12]. With the advancement of electrospinning technology, various types of electrospinning membranes, such as random, align, lattice etc., have been developed [13]. Of these, the aligned electrospinning membranes have a wide range of applications in the field of skin tissue engineering [1,14,15], since they can provide a series of biologically chemical and physical cues for regulating cell behaviors and transmitting mechanical and electrical fields [16]. The aligned topography of electrospinning membranes has recently been of great interest due to the similarity to the arrangement of fibroblasts and smooth muscle cells in most soft tissues. For example, studies have corroborated that more elongated fibroblasts shaped by the aligned topography expressed higher collagen type I than less stretched cells and revealed that elongated cells in vivo, had optimal morphology in terms of expression of collagen type I [17]. Another study has been reported that fibroblasts can migrate for a long distance in a highly correlated manner at a constant speed on the aligned electrospinning membranes [18], in which it is more convenient to frequently assemble and disassemble the focal adhesion responsible for potent cell motility source. The cells attached to the radially aligned nanofibers can more

efficiently migrate from the surrounding healthy tissue to the central injured site along the topographic clues, so as to promote wound healing [19].Critically, aligned electrospinning membranes could promote the normal differentiation and outgrowth of vascular smooth muscle cells and be used constructing blood vessels in tissue engineering [14,20]. Even though already widely used as skin tissue engineering biomaterials, the aligned electrospinning membranes are still verified with poor inflammation resistance and mechanical properties [21], which obviously impede its wider application. Many studies have attempted to improve physicochemical properties and biological performance of the aligned electrospinning membranes via adjusting their microstructure, since topographical factors indeed exert some indispensable roles in early cell fate prior to cytokines [22]. In view of the fact that the ECM is composed of different fibers from nano to micron, the diameter factor dictating the physicochemical properties and biological performance of electrospinning membranes was introduced [23]. For example, human skin fibroblasts had a well-diffused morphology, growing on the electrospinning fibrous matrix of the range of 350-1100nm diameter, where the expression of type III collagen gene in human skin fibroblasts was significantly up-regulated [24].When human dermal fibroblasts were seeded on electrospinning poly (methyl methacrylate) scaffolds with different diameters, it was found that there was a critical minimum diameter (d), namely 0.97μm, making the fibroblasts better directionally developing in contrast to d<0.97μm [25]. Additionally, the electrospinning bio-scaffolds composed of bombyx mori silk fibroin fiber with the small diameter (about 250-300nm) had stronger support for the dermal fibroblast proliferation than that with the diameter of about 1μm [26]. It has been reported that the diameter of electrospinning bio-scaffolds could affect the immune response of macrophages, especially in the early stage of inflammation since nanofiber poly-L-lactic acid scaffolds minimized inflammatory response relative to microfiber scaffolds [27]. Studies involving fibroblasts and macrophages have corroborated the positive effect of diameter factor of electrospinning membranes on cell behavior. However, the specific characteristics of these electrospinning membranes as to which diameter interval is most suitable for skin tissue

engineering have not been conclusive. And this part on *in vivo* research has not been explored. Herein, this article innovatively explores the skin defect response to aligned fish collagen reinforced Poly (lactide-co-glycolide) electrospinning membrane (FC/PLGA) with varying fiber diameters including 319±100nm (A300), 687±138nm (A600) and 1048±130nm (A1000) [28,29], to develop a more suitable surface wound healing medical device for promoting the re-epithelialization with appendages. This comprehensive study also evaluated the transcriptome of rat skin wounds on the FC/PLGA membrane of varying fiber diameters for exploring the potential diameter-mediated mechanism of repairing tissue defects.

2. Experimental Section

2.1. Materials. Poly (lactide-co-glycolide) (PLGA, LA/GA = 75:25, Mw = 105kDa, dispersity is 1.897) was purchased from Jinan Daigang Biomaterial Co., Ltd. (Shandong, China). Fish collagen (FC) from fish scale and skin was procured from Sangon Biotech Co., Ltd. (Shanghai, China). 1,1,1,3,3,3-Hexafluoro-2-propanol (HFIP), N-hydroxysuccinimide (NHS), and 1-ethyl-3-(3-dimehylaminopropyl) carbodiimide hydrochloride (EDC) were offered by Aladdin Co., Ltd. (Shanghai, China).

2.2. Electrospinning. To prepare the aligned fish collagen reinforced Poly (lactide-co-glycolide) electrospinning membrane (FC/PLGA) with different diameters, PLGA and FC were dissolved in HFIP under stirring at 25°C. The solution was stirred vigorously until complete dissolution of PLGA and FC. Subsequently, the prepared electrospinning solutions were employed to fabricate fibrous aligned membranes with different diameters via electrospinning. The electrospinning solutions were loaded into a plastic syringe fitted with a flat-tipped 21G stainless steel needle. A high voltage and a distance were applied between the needle and the roller collector of 2800rpm covered with a piece of aluminum foil. The solution was fed at a constant speed, regulated by a precision syringe pump (The electrospinning parameters were shown in **Table S1**. The preliminary experiments were shown in the **Figure S1**). The prepared

electrospinning membranes were dried in a vacuum oven at 25 °C until the solvent was completely volatilized, which was confirmed by **FTIR** spectra (**Figure S2**).

2.3. Characterization. Scanning electron microscope (SEM; JEOL, JSM-6510LV, Japan) was employed to observe the morphology of the aligned electrospinning membranes with different diameters. In addition, Image-Pro Plus was applied to quantitatively measure the randomly selective 200 fiber diameter, distribution and alignment (orientation < 10°) [30], from the SEM images obtained. To estimate the mechanical performance of these membranes, the samples were attached to an electronic universal testing machine (SHIMADZU, AG-IC 50 KN, Japan) with a 50-N load cell. Prior to testing, the samples of thickness 0.1−0.2mm were cut into a dumbbell shape having a gauge length of 75mm and width of 4mm. Five samples were measured for each diameter of membrane. The tensile properties of membranes were determined under a constant upper clamp speed of 5mm/min at room temperature in accordance with the criteria of'Plastics-Determination of tensile properties of films'(GB/T 1040.3−2006, corresponding with ISO 1184−1983). The elastic modulus was calculated from the slope of the linear region (ε = 1−3%) of the tensile-stress curve. **Atomic force microscope** (AFM; JEOL, JSM-6510LV, Japan) was employed to observe the roughness of the aligned electrospinning membranes with different diameters. The surface wetting behavior of the membranes was characterized by measuring the water contact angles by using a contact angle measuring instrument (Chengde Dingsheng, JY-82B, China) and hydrophilicity test. Five samples were tested for each type of membrane to obtain an average value.

2.4. In Vitro Swelling and Degradability Study. The aligned electrospinning membranes with different diameters were immersed in 50mM of EDC/NHS and 10mM of MES ethanol solution for 24h at 4°C. The membranes were washed three times with ethanol and then dried in vacuum oven for 24h. The dried fibrous membranes were cut into squares of side 10mm and weighed accurately; then, they were put into a 5mL plastic tube with 4mL of PBS solution (pH = 7.4). Subsequently, all tubes were put in a shaking incubator at 100rpm and 37°C. The remaining incubating

media were changed every week. At each predetermined time point, the samples were dried to a constant weight in a vacuum oven. The swelling and weight loss rate were calculated according to the following formula:

Weight remaining (%) = $m / m_0 \times 100\%$

Where m_0 is the mass of membranes before incubation and m is the mass of membranes after incubation for different time.

2.5. *In Vitro* Cell Culture Experiments. 2.5.1. Cell Culture and Seeding. The fibroblasts (L929) and human oral keratinocytes (HOK) were obtained from West China School of Stomatology, Sichuan University. The extraction was according to the normative procedure, which was approved by the Ethics Committee of Sichuan University. The L929 and HOK were cultured in RPMI medium modified (1640; Gibco, USA) supplemented with 10% fetal bovine serum (FBS, Gibco, USA) and a 1% mixture of penicillin/streptomycin (MP Biomedicals, USA). The culture medium was replaced every other day in both the L929 and HOK culture cycle. These membranes were preprocessed by immersing in a 75% ethanol solution for 0.5h. Subsequently, all the prepared membranes were sterilized by γ-irradiation for cell experiment. The L929 and HOK cells (2×10^4 cells/well, respectively) were seeded and incubated separately at 37°C with 5% CO^2 atmosphere.

2.5.2. Cell Proliferation and Morphology. The proliferation of L929 and HOK on these membranes were assessed by cell counting kit-8 (CCK-8, DOJINDO, Japan) assay. The optical density (OD) value was read by a 1420 Multilabel Counter (PerkinElmer, USA) at 450nm. The percentage of dead cells was stained with propidium iodide (PI), according to the product instructions (DOJINDO, Japan). Fluorescence images were visualized with an inverted fluorescence microscope (Leica, Germany). Scanning electron microscopy (SEM; JEOL, JSM-6510LV, Japan) was employed to observe the morphology of cell on the electrospinning membranes.

2.6. *In Vivo* Animal Experiments. Sprague−Dawley (SD) rats aged 8 weeks with an average weight of 220g were

obtained from the experimental animal center of Sichuan University approved by the Ethics Committee of Sichuan University. The experimental rats could touch feed and tap water at will. The healthy status of the rats was checked every day during the experimental period. After conventional fasting for 12h, the experimental rats were intraperitoneally anaesthetized in accordance with the instructions of the Animal House. Subsequently, a circular defect of diameter 6mm was created on the right and left skin of the dorsum via surgery following skin preparation. After transplanting different diameter aligned electrospinning membranes, the skin wounds were covered with 3M™Tegaderm™ and fixed on the latex ring with 3.0 silk suture. The experimental rats should receive routine postoperative nursing [31]. The experimental rats were divided into four groups with randomness: Ctr (skin wounds transplanted with the saline); A300 (skin wounds transplanted with A300 electrospinning membranes); A600 (skin wounds transplanted with A600 electrospinning membranes) and A1000 (skin wounds transplanted with A1000 electrospinning membranes). The rats were executed 5, 7 and 14 days after surgery with the excess anesthetic followed by inhaling CO_2. The skin wounds of rats were extracted for general analysis. All tissue sections were obtained from the rat skin wounds for routine histological examination and stained with Masson's trichrome staining (MST Staining). And the thickness of fibrous capsule was determined manually under a microscope, using 5 randomly picked fields (at 100 magnification) of the Masson's sections for evaluating the foreign body reaction. Immunohistochemistry (IHC) was performed for CD31 (ab182981, Abcam, 1:2000) to evaluate the vascularization. Double staining immunofluorescence (IF) was performed for cytokeratin 5 (K5, ab52635, Abcam, 1:200) and cytokeratin 10 (K10, ab76318, Abcam, 1:150) to evaluate the keratinization. Both were further verified by quantitative reverse transcription-polymerase chain reaction (qRT-PCR), of which the data were presented as the relative quantification (RQ) compared with control groups (The related primers were shown in Table 1).

Table 1. Sequences of Primers Utilized in the Study

Gene	forward primer (5′-3′)	reverse primer (5′-3′)
CD31	GGTAATAGCCCCGGTGGATG	TTCTTCGTGGAAGGGTCTGC
CD68	TGGGGCCTCTCTGTATTG	TCTGATGTCGGTCCTGTTT
GAPDH	AGTGCCAGCCTCGTCTCATA	GATGGTGATGGGTTTCCCGT
K5	GCCTCCTCCAGCTCAGTC	AAGAAGCAGTGTGCCAACC
K10	TACGAGAAGCACGGCAA	GGCATTGTCAGTTGTCAGG
IL-10	AGGGTTACTTGGGTTGCC	GGGTCTTCAGCTTCTCTCC
MMP12	CTCCCATGAACGAGAGCGAA	GGTGTCCAGTTGCCCAGTTA
TGFβ	AGGGCTACCATGCCAACTTC	CCACGTAGTAGACGATGGGC

2.7. Transcriptome Analysis. Three replicates of rat skin wounds in each group were detected for the assay of transcriptome, and the results were analyzed for Gene Ontology (GO) and Kyoto Encyclopedia of Genes and Genomes (KEGG) for screening the related targets. These were further verified by fluorescence quantitative PCR (The related primers were shown in **Table 2)** and enzyme linked immunosorbent assay (ELISA).

2.8. Statistical Analysis. At least three independent assays were conducted to obtain repeatable data if not distinctively explained, and the data was dealt with Case Viewer, Origin 2019 or Graphpad Prism 8.0 software. Statistical analyses were performed by Student's t-test and one-way analysis of variance test. The numerical data are presented as mean ± standard deviation. A value of $p < 0.05$ was considered statistically significant (*$p < 0.05$, **$p < 0.01$, ***$p < 0.001$).

3. Results and Discussion

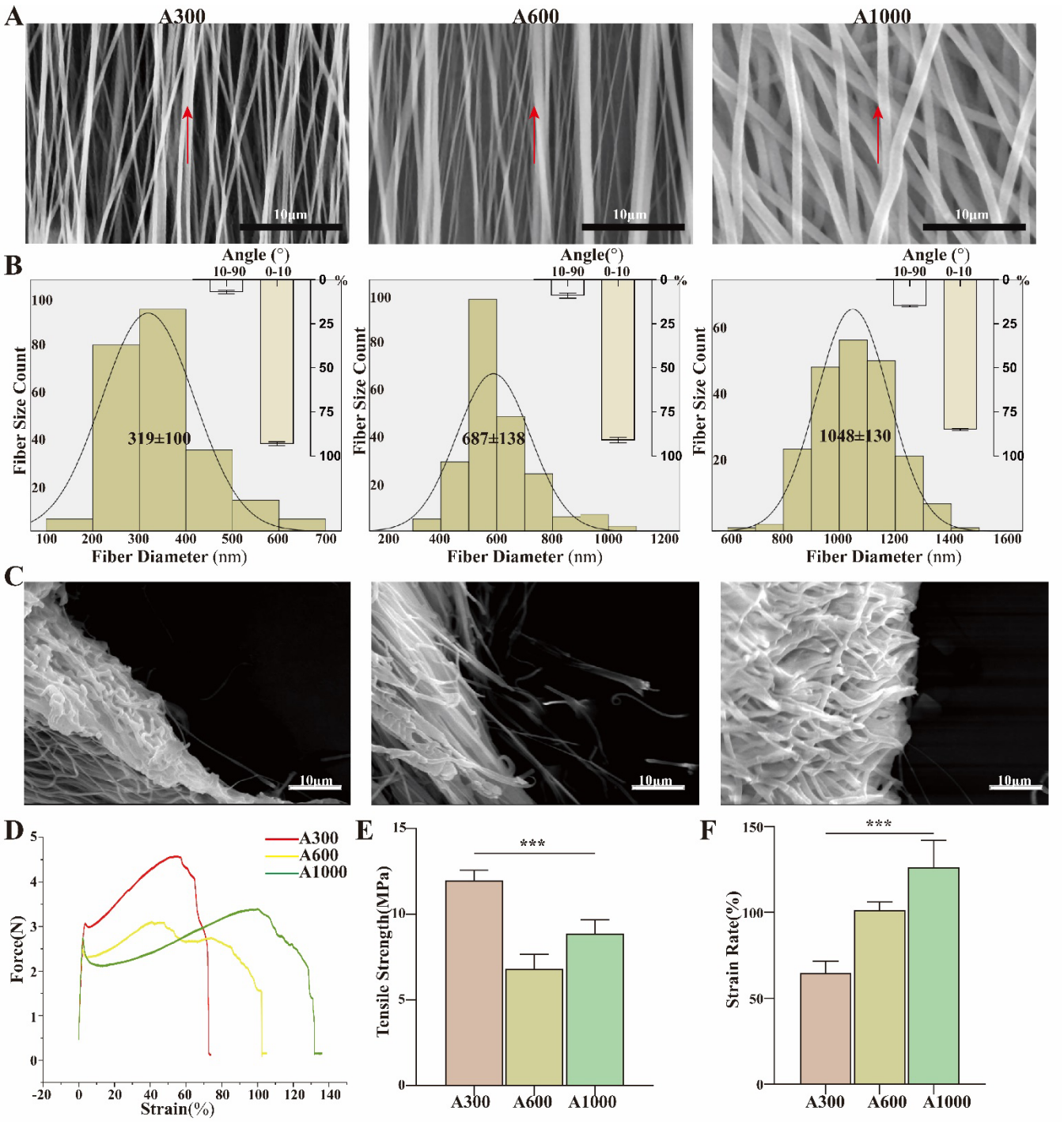

Figure 1. (A) SEM images and (B) corresponding diameter distributions of different diameter aligned electrospinning membranes; (C) SEM images of tensile test and (D) typical stress−strain curves of various membranes; (E) tensile strength; (F) strain rate.

3.1. Topological and Mechanical Properties. The topology and corresponding fiber diameter distributions of the

electrospinning membranes are shown in **Figure 1A** and **1B**, revealing that the fibers presented a homogeneously bead-less performance, and a highly aligned morphology. Based on the histogram of **Figure 1B**, the mean diameter of fibers was reduced obviously with the change of operation and solution parameters. This is mainly because the increase of electric field promoted the stretch rate of electrospinning fibers and the decrease of PLGA restrained the electrospinnability itself (**Table 1**), resulting in the electrospinning fibers with a narrower size distribution and smaller mean diameter [26]. It is typically considered that submicron-scaled electrospinning bio-scaffolds possess better pro-healing effect for tissue engineering since the main advantage of submicron-scaled features over micron-scaled features is that they both provide a larger surface area to adsorb proteins and form more adhesion sites to integrin [32,33]. The mechanical performance of electrospinning membranes is an important determinant for its application in wound healing, which is expected to present suitable mechanical strength during surgery and tissue regeneration. In this research, we evaluated the mechanical behaviors of different electrospinning membranes (before cross-linking) via tensile strength tests. The stress−strain curve (**Figure 1C** and **1D**) illustrates that the tensile strength of small diameter aligned electrospinning membrane (A300) increased compared with medium diameter (A600) and large diameter (A1000), as presented in **Figure 1E**. Meanwhile, the strain rate of A300 maintained a lower level (**Figure 1F**), apparently increasing the mechanical stability of this electrospinning membrane, which could prevent scars in skin wound healing [34]. The mechanical performance of these electrospinning membranes could be partially explained by the fracture process of fibers. This is primarily because membranes comprising smaller diameter fibers performed both higher strength and lower ductility [35,36].

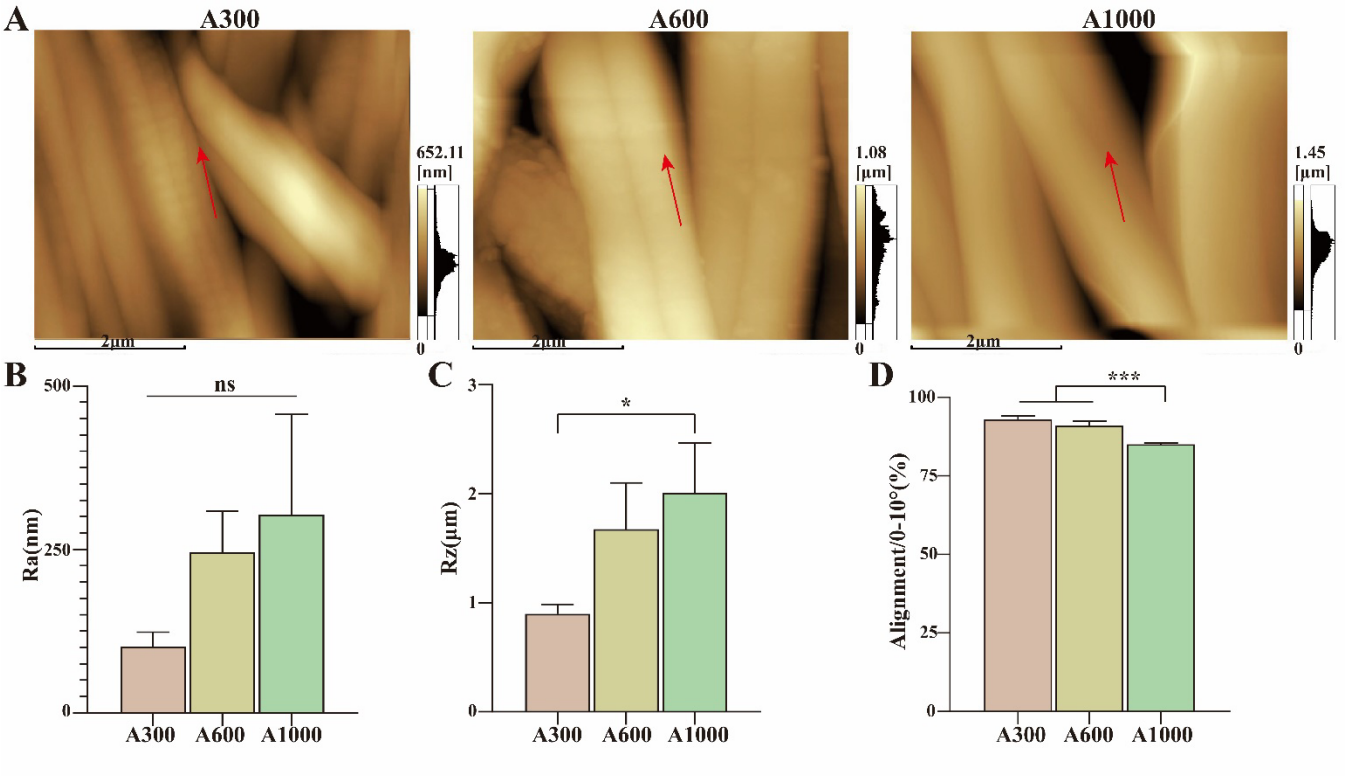

Figure 2. (A) AFM images and (B-C) corresponding roughness analysis of different diameter aligned electrospinning membranes; (D) alignment analysis of various membranes.

3.2. Roughness and Physicochemical Properties. As shown in **Figure 2A-C**, the roughness of electrospinning membranes seemed to be increased with the increase of mean diameter itself, which is consistent with the abovementioned result of SEM and beneficial for cell adhesion and migration to some extent [37]. Nevertheless, this trend is not statistically significant difference. These electrospinning membranes possess high specific surface area, thus providing larger surface area for cell adhesion as contrast to 3-dimentional scaffolds fabricated using other techniques. The high surface area could prevent undesirable fluid accumulation and accommodate more facile oxygen permeation [38]. It has been reported that membranes with fibers arranged in parallel (alignment) are beneficial to the normal differentiation of vascular smooth muscle cells, and have more potential to be applied to the construction of tissue-engineered blood vessels [14]. In this study, the alignment of A300 was similar to that of A600 yet much stronger

than that of A1000, indicating its potential of vascularization (**Figure 2D**).

3.3. Wettability and *in Vitro* Degradation Behavior. The wettability of the electrospinning membranes was investigated by water contact angle (WCA) assay. As shown in **Figure 3A**, the electrospinning membrane of A300 exhibited a water contact angle of 58.52°, resembling that of A600 (54.15°) yet less than that of A1000 (83.69°), which demonstrated its hydrophilic behavior. It was evident that the decrease of fiber diameter significantly increased the water affinity of electrospinning membranes. This is mainly because the high specific surface area conveniently interacts with water molecules. The morphology of material directly influences hydrophilicity of the material thereby dictating the WCA. Apart from the fiber diameter, the fiber arrangement and surface roughness of electrospinning membrane exert significant influence on hydrophilicity of biomaterial. We further studied the wettability behavior by evaluating the infiltration of these three electrospinning membranes. As was evident from **Figure 3B**, the electrospinning membrane of A300 was completely wetted, marginally better than that of A600 (97.86%) yet significantly better than that of A1000 (47.54%), consistent with the aforementioned result of WCA. An ideal implanted biomaterial such as a guided tissue regeneration (GTR) membrane should have both suitable mechanical strength as well as matched biodegradability. Fiber degradation gradually destroys the structural and functional integrity of electrospinning membranes. For evaluating the in vitro degradability of the assayed membranes, we monitored the remaining mass during the immersion process. As shown in **Figure 3D**, the degradation rate of A300 was significantly higher than those of the others at all the time points. The results showed that the decrease of diameter altered the degradation behavior of fibers, thereby accelerating the degradation of the composite fibers.

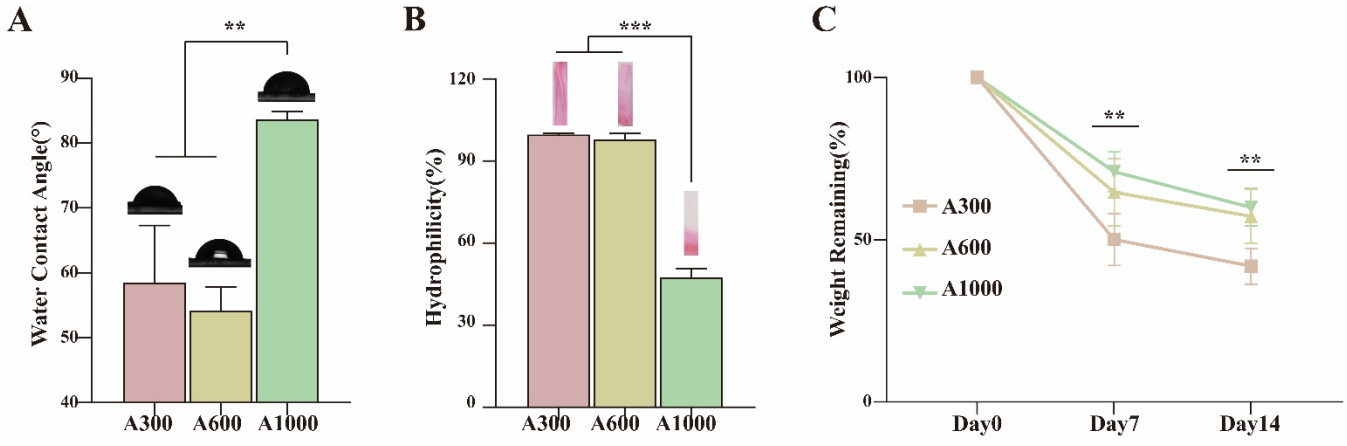

Figure 3. (A) WCA images and corresponding analysis of different diameter aligned electrospinning membranes; (B) hydrophilicity images and corresponding analysis of various membranes; (C) degradation assays.

3.4. Cell Biocompatibility Behavior. Before clinical application, the different diameter aligned electrospinning membranes utilized for GTR should be considered to perform the ability for ameliorating related cell proliferation and/or migration. Accordingly, the proliferation of L929 and HOK on different diameter aligned electrospinning membranes was assessed, as shown in **Figure 4A** and **4B**. For L929, the proliferation rate of A300 was significantly higher than those of the others except for control group at all the time points. However, there was no statistically significant difference between groups of HOK proliferation. The results indicate that the small diameter membranes were more conducible for the proliferation of L929 yet seemed to have no significant influence on that of HOK [39]. It is reported that the cell performance on membranes are intimately related with fiber diameter and topological structure, directly manipulating the cell adhesion and exchange of nutrients [24,26,27] . The fiber diameter of the aligned electrospinning membranes decreased from 1048 ± 130 nm to 319 ± 100 nm with the change of operation and solution parameters, which could result in the promotion of cell adhesion and proliferation of A300 [40]. In order to deeply explore the effect of different diameter aligned electrospinning membranes on HOK, we further studied the viability and morphology of HOK via the fluorescent staining of PI and SEM. As shown in **Figure 4C** and **4D**, the dead HOK

on electrospinning membrane of A300 (33.0) was marginally less than that of A600 (34.3) and A1000 (36.0) on day 3, but didn't reflect statistically significant difference. Additionally, as presented in **Figure 4E**, the result of SEM revealed that the HOK spread on the electrospinning membrane of A300 much better than that of A600 and A1000 on day 1, consistent with previous studies that cells adhered on nanofibers much better than microfibers[41]. Overall, it may have different degrees of positive effects on different types of cells, such as promoting L929 proliferation and accelerating HOK spread, respectively. Our results also indicate that the surface properties of the membrane including diameter, wettability and roughness seemed to manipulate the biological behavior of L929 and HOK [42,43].

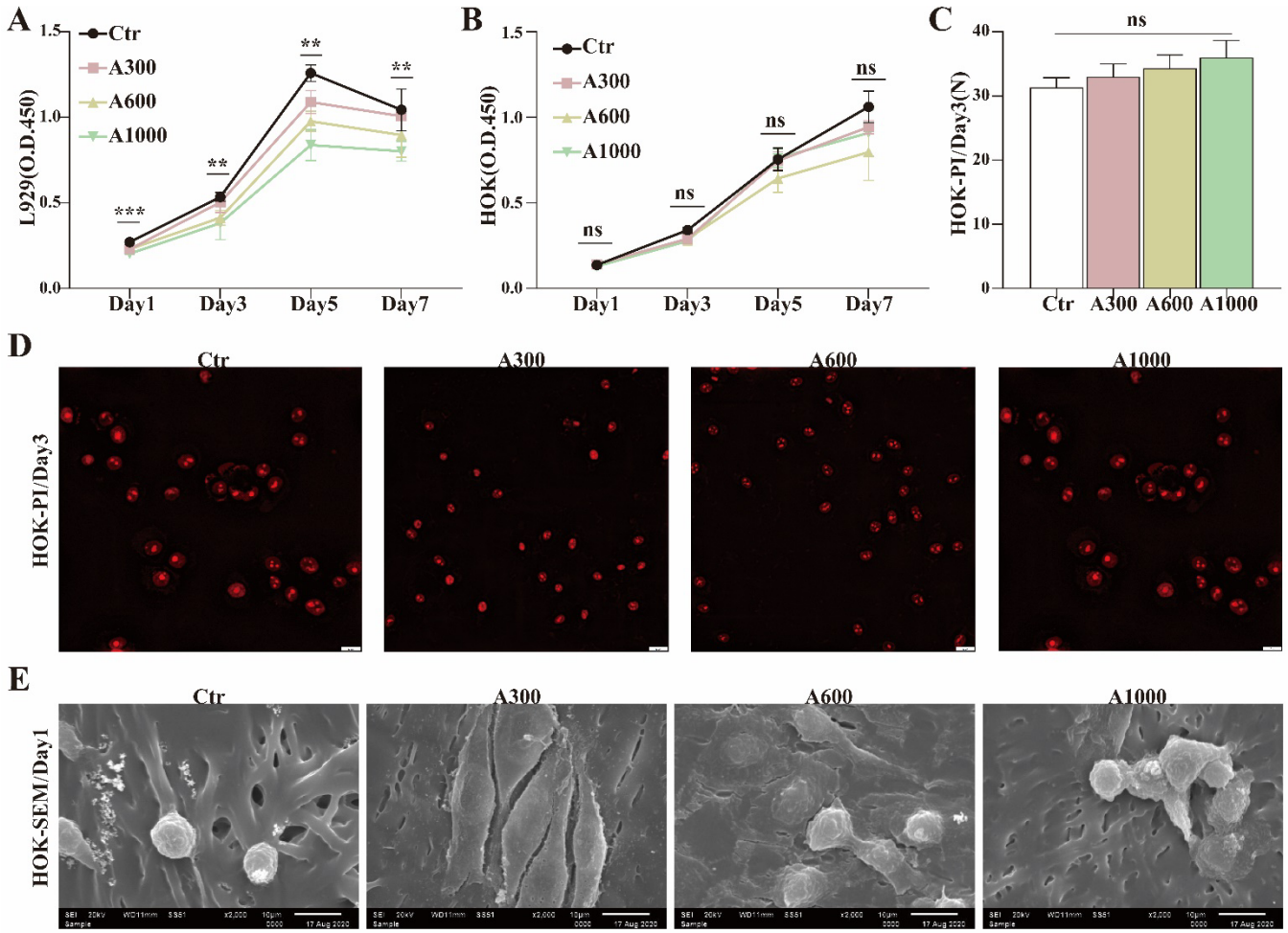

Figure 4. CCK-8 tests of (A) L929 and (B) HOK; (C) analysis and (D) corresponding images of PI fluorescent staining of HOK; (E) SEM images of HOK morphology.

3.5. *In Vivo* Restoration Performance. In practical application, these membranes utilized for GTR could be recognized to present the ability for accelerating related wound healing. Accordingly, the restoration performance of skin defect of rat on different diameter aligned electrospinning membranes was assessed, as shown in **Figure 5A** and **5B**. For rat skin defects, the residual area of A300 group was significantly smaller than those of the others at all the time points. Intriguingly, the wounds in A300 group occasionally reached the complete healing one or two days earlier. The macroscopic result indicate that the small diameter membranes were indeed more conducible for the restoration of rat skin defects, completely consistent with the aforementioned results of cells *in vitro*. We further studied the wound healing by evaluating the hematoxylin and eosin (H＆E) staining of tissue sections. As was evident from **Figure 5C** and **5d**, the residual gap of A300 group (2.70mm) was significantly narrower than that of A600 (3.63mm) and A1000 (4.15mm) on day 7, confirming the previous macroscopic result that rat skin defects of A300 closed faster.

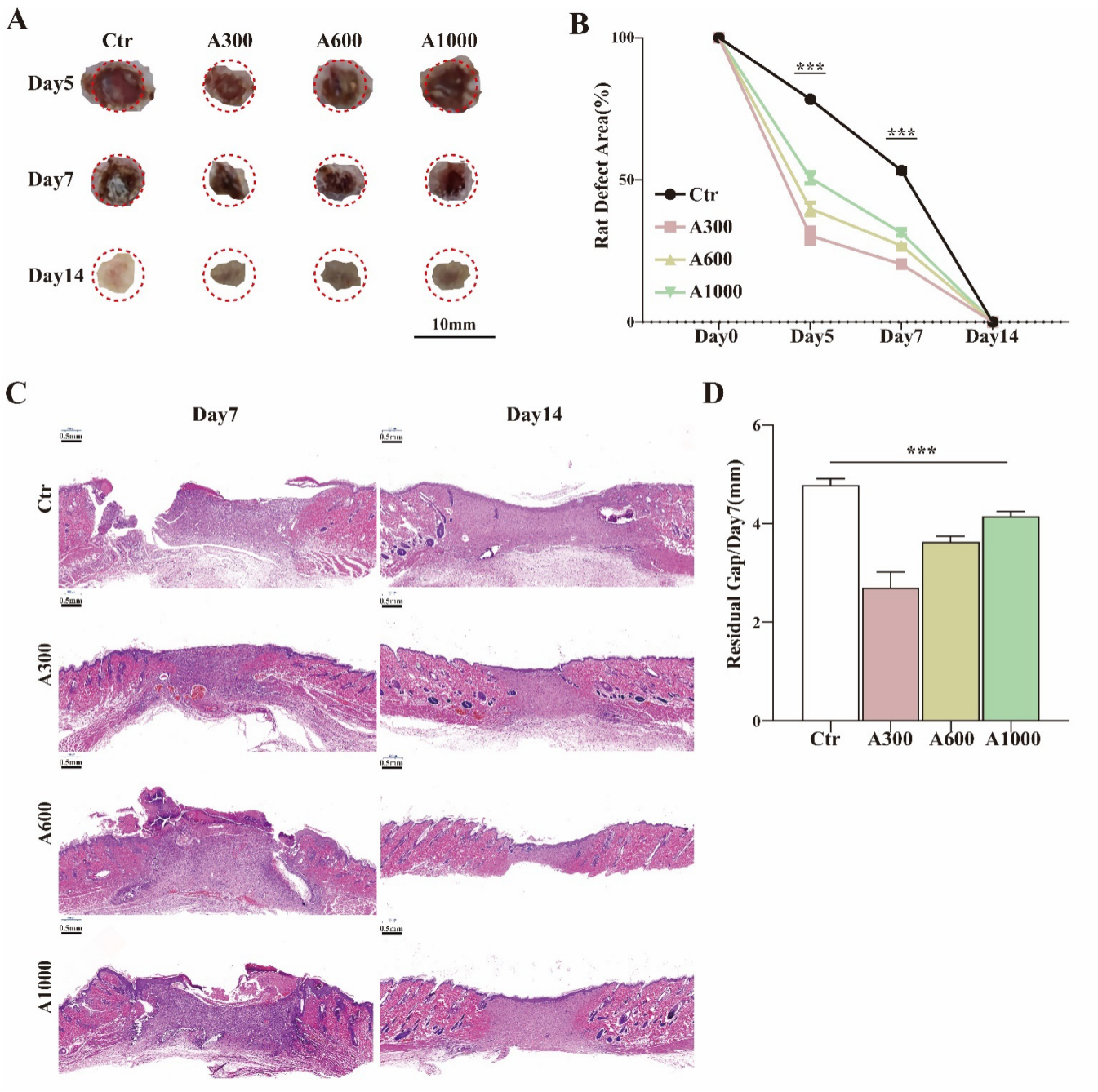

Figure 5. (A) Macroscopic images of rat skin defects and (B) corresponding analysis; (C) residual gap images of H＆E of rat skin defects and (D) corresponding analysis.

Additionally, the keratinized layer of wounds first appeared in A300 group yet didn't exist in other groups on the 7th day after operation. There was no significance between control and various diameter groups on day 14, whereas the thickness of keratinized layer in A300 group was closer to that in control group (**Figure 6A**), as further corroborated by

the RNA expression of K5/K10 (**Figure 6B** and **6C**) and corresponding immunofluorescence staining (**Figure 6E**), both revealing that the degree of epithelization of A300 group was significantly better than other groups. It has been reported that hair follicle stem cells could accelerate wound healing as well as tensile strength [44]. And the maximum number of newly-formed hair follicles on day 14 (**Figure 6D**) was presented in A300 group, demonstrating that A300 group achieved excellent repair results with regenerated appendages [45].

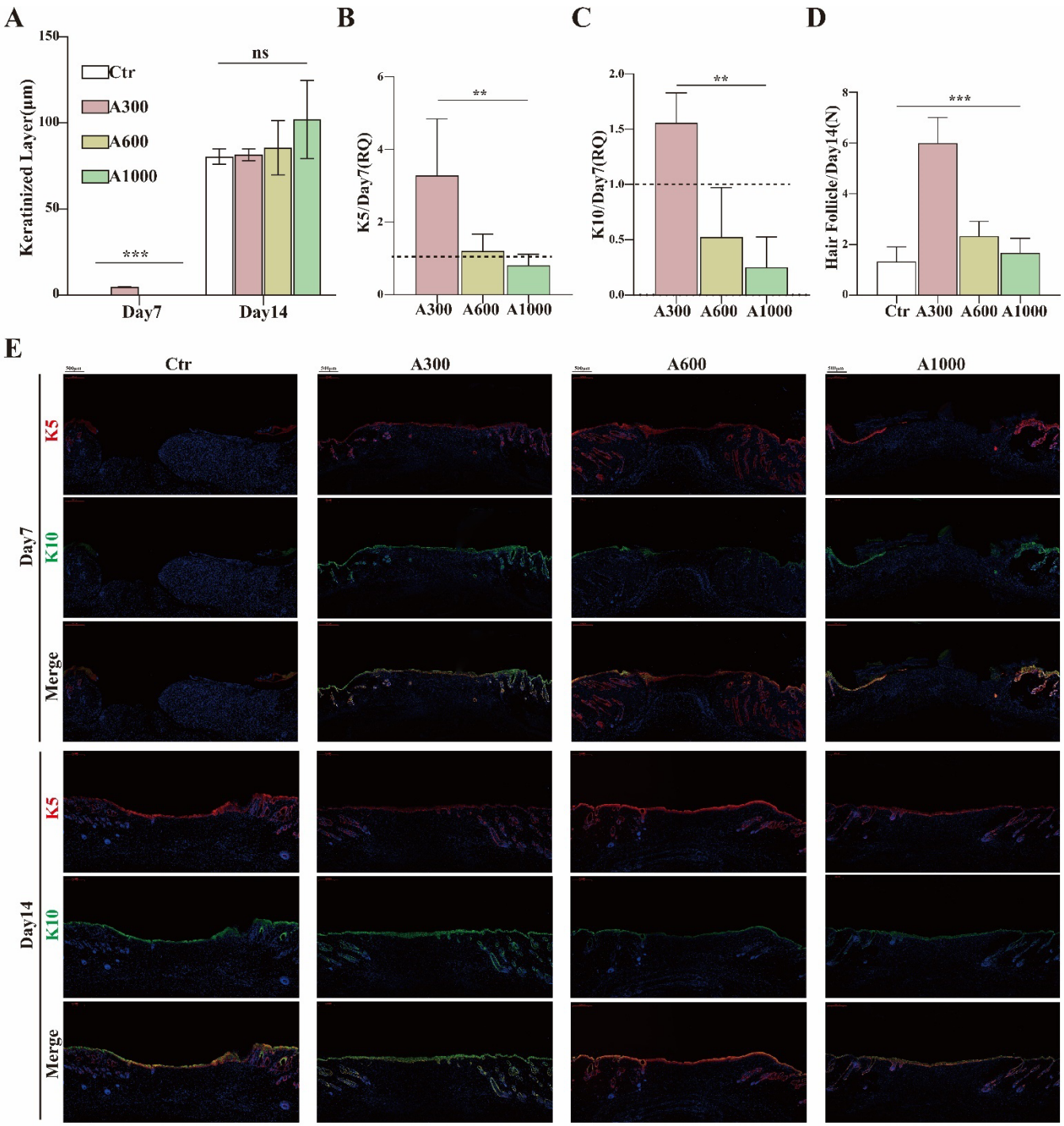

Figure 6. (A) The analysis of keratinized layer images of H＆E of rat skin defects; (B) The RNA expression of K5; (C) The RNA expression of K10; (D) The number of regenerated hair follicles on day 14; (E) K5(red)/K10(green)-positive images of immunofluorescence staining of rat skin defects.

It's well known that the newly formed blood vessels could provide the necessary nutrients utilized for promoting wound healing [46]. Based on images of **Figure 7A** and **7B**, the result indicated that the degree of vascularization of A300 group (0.250mm^2) was significantly greater than that of A600 (0.125mm^2) and A1000 (0.080mm^2) on day 7, as further demonstrated by the dominant RNA expression of CD31 (**Figure 7C**) and corresponding of immunohistochemical staining in A300 group (**Figure 7D**). It is so concluded that the A300 group played a more important role in both epithelization and vascularization, suggesting that aligned electrospinning membranes of A300 indeed accelerated wound healing of rats.

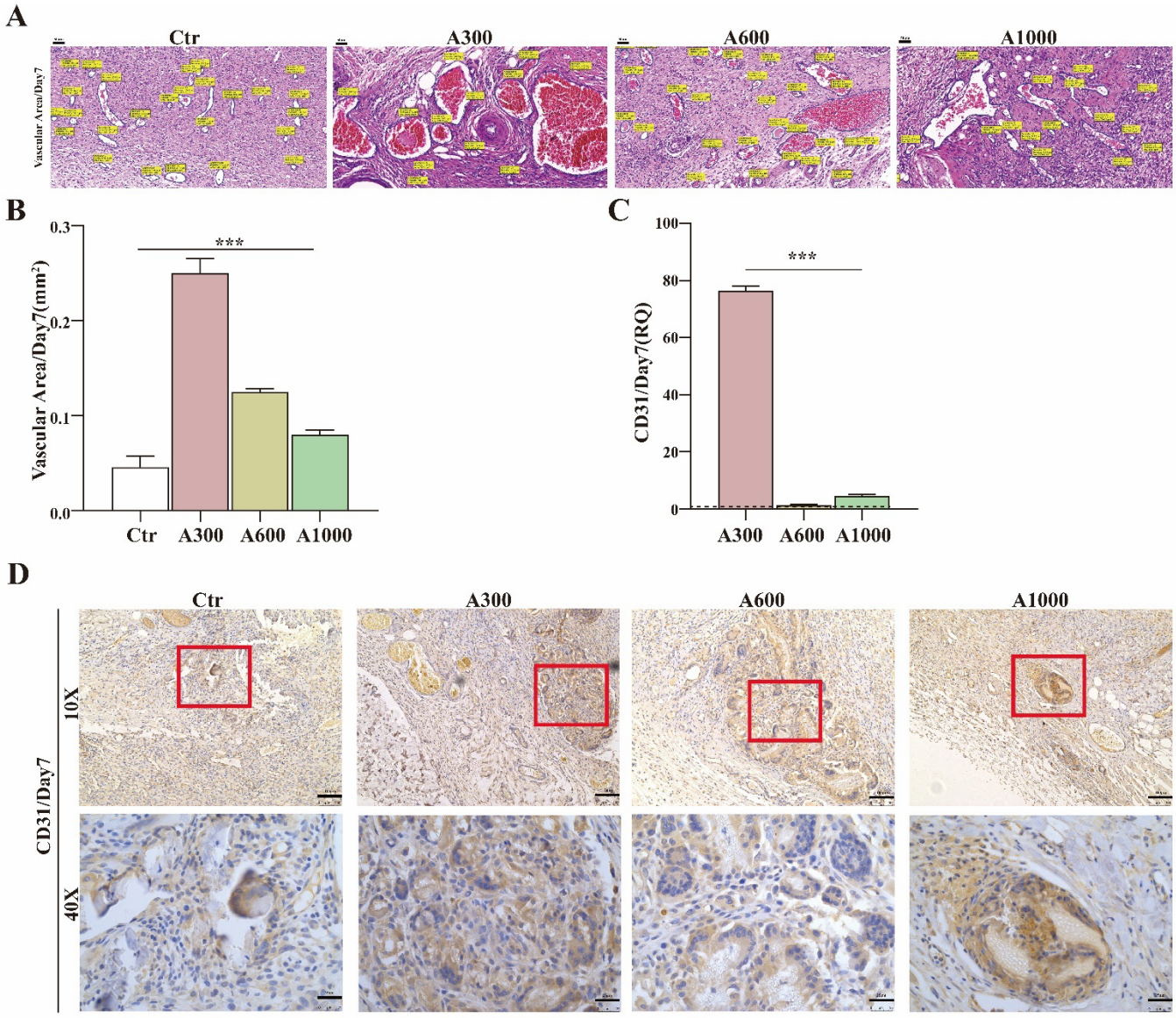

Figure 7. (A) Vascularization images of H & E of rat skin defects and (B) corresponding analysis; (C) The RNA expression of CD31; (D) CD31-positive images of immunohistochemical staining of rat skin defects.

For many wound applications, the performance of electrospinning membranes is built on its friendly interaction with the host immune defense system[47], since the immune recognition initiates foreign body reactions (FBR) comprising continuous inflammation, fibrosis (fibrous capsule) and damage to the neighbouring tissue[48,49]. These unwanted outcomes can both destroy the function of electrospinning membranes and arise obvious pain and discomfort for the recipient [50].In this study, the macroscopic result of rat skin defects showed that there seemed to be better wound

healing and less scar tissue in the A300 group on day 14 (**Figure 5A**).We further studied the thickness of fibrous capsule of rat subcutaneous implantations via the MST Staining to evaluate the degree of FBR. As depicted in **Figure 8A** and **8B**, the thickness of fibrous capsule of A300 group (12.40μm) was significantly thinner than that of A600 (43.65μm) and A1000 (71.66μm) and reflected statistically significant difference. Additionally, the number of immune cells recruited by electrospinning membranes of A300 and A600 was less than that of A1000 (**Figure 8C** and **8D)**. It's so concluded that electrospinning membranes of A300 could friendly interact with the host immune defense system and marginally give rise to the FBR for reaching the normal healing. Other researchers have described that nanofiber scaffolds minimized inflammatory response relative to microfiber scaffolds [27].However, the specific mechanism of reducing inflammation/FBR remains unclear.

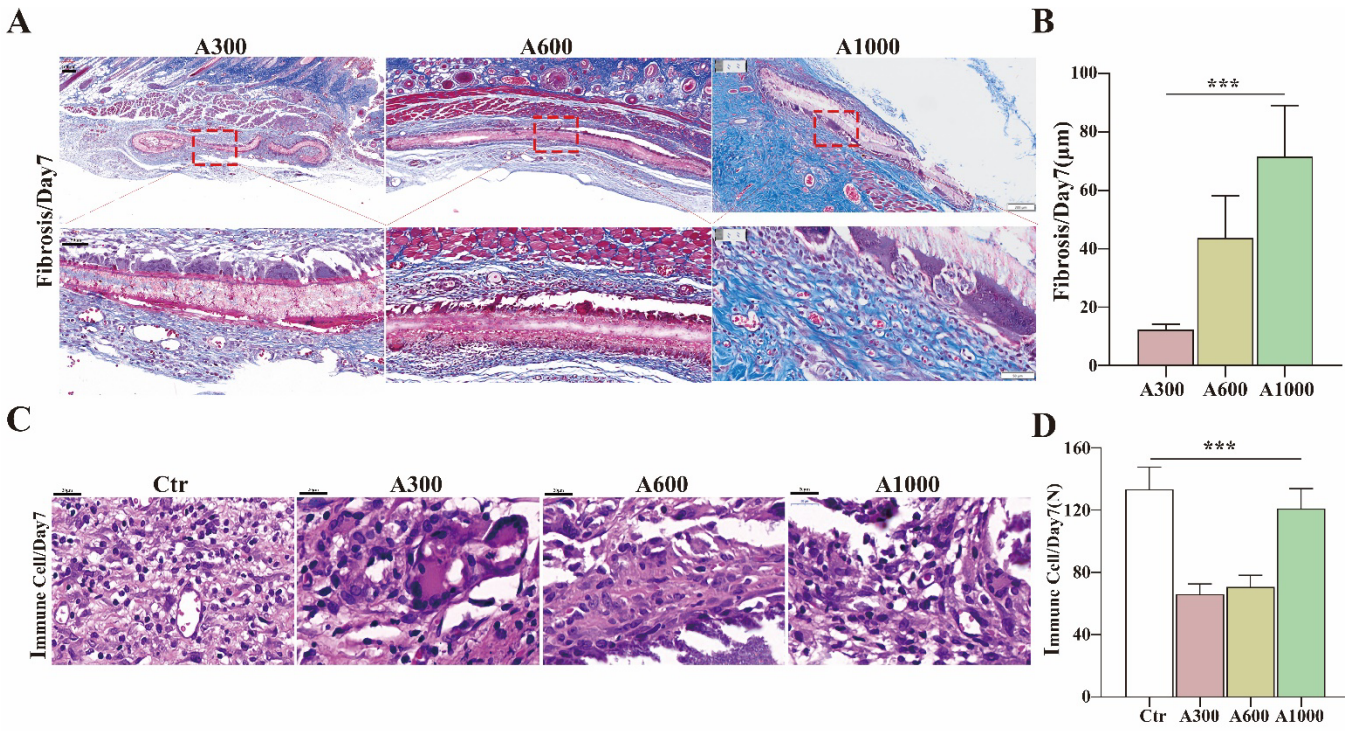

Figure 8. (A) FBR images of Masson staining of rat subcutaneous implantations and (B) corresponding analysis; (C) inflammatory cell infiltration images of H & E of rat skin defects and (D) corresponding analysis.

3.6. Transcriptome Analysis. In order to further explore the specific mechanism of reducing inflammation/FBR for the better wound healing, the transcriptome of rat skin defects implanted with different diameter aligned electrospinning membranes was studied via the principal component analysis (PCA), Gene Ontology (GO) and Kyoto Encyclopedia of Genes and Genomes (KEGG) to screen the inflammation-related targets. The results of PCA showed that A300 was obviously different from other experimental and control groups (**Figure S3A**), suggesting that the diameter factor indeed played an important role in wound healing. As presented in **Figure S3B-D**, the results of GO showed that the significantly up-regulated biological process (BP) items of A300 primarily included immune-related processes, such as *positive regulation of immune response* and *innate immune response*, relative to control and A1000 groups. However, compared with A600, the significantly up-regulated BP items of A300 was angiogenesis- and extracellular matrix-related process, this was probably because the difference of wound healing between A300 and A600 was smaller. After that, the genes of immune-related processes that displayed significant changes were chosen and presented as heat maps. From the heat maps (**Figure 9A and 9B**), we learned that the expression of A300 was similar to that of A600 yet much stronger than that of control and A1000 in the abovementioned immune-related process, indicating that A300 could reduce inflammation/FBR probably by actively regulating immune response for achieving better wound healing. It has been reported that matrix metalloproteinases 12 (MMP12) actively regulates the proliferation, diffusion and migration of epidermal cells and protects against corneal fibrosis via regulating immune cell infiltration and angiogenesis in the process of corneal wound healing [51,52] . In this study, the significantly differentially expressed MMP12 appeared both in *positive regulation of immune response* and *innate immune response* of rat skin defects. For this reason, we evaluated the RNA and protein expression of MMP12 of rat skin defects implanted with different diameter aligned electrospinning membranes through ELISA. The RNA and protein expression of MMP12 of A300 was indeed higher than other groups and reflected statistically significant difference (**Figure 9C** and **9D)**,

suggesting that MMP12 may likewise promote the proliferation, diffusion and migration of epidermal cells in skin wound healing. It's usually considered that MMP 12 is predominantly expressed by macrophages [53] .Accordingly, the macrophage-related genes that displayed significant changes were chosen and presented as heat maps. From the gene heat maps (**Figure 9E** and **9F**), we acquired that the expression of A300 on reparative macrophages (M2) was similar to that of A600 yet much stronger than that of control and A1000. Nevertheless, the expression of A300 on inflammatory macrophages (M1) was much weaker than that of other groups. The results of RNA expression on Cd68, IL-10 and TGFβ (**Figure 9G**) also showed that A300 was much stronger than other groups, corroborating that electrospinning membranes of A300 indeed promoted macrophages transforming to M2. It has been reported that M1 could inhibit keratinocyte migration [54,55]. Furthermore, the migration ability of HOK stimulated by the conditioned medium derived from Thp1 inoculated on electrospinning membranes of A300 was the strongest (**Figure S4**). The phagocytosis, as a process for maintaining cell homeostasis and organelle renewal, is a pivotal factor in inducing macrophages to reprogram from pro-inflammatory M1 phenotype to pro-healing and pro-resolving M2 phenotype during the wound healing, as alternatively activated pathways play little role in M1-M2 reprogramming in vivo [56,57]. As for this research presented in **Figure S5A-C**, the results of KEGG showed that the significantly up-regulated signal pathways items of A300 primarily included *lysosome* and *phagosome*, relative to control and A1000 groups. The heat maps derived from *lysosome* and *phagocytosis* items (**Figure S5D** and **S5E**) also presented genes related to phenotype transformation of macrophages. Additionally, the autophagy marker, LC3B of IHC staining of rat skin defects (**Figure S5F**) corroborated the above outcomes of gene heat maps. It is so inferred that electrospinning membranes of A300 group could promote macrophages transformation to M2 through phagocytosis, subsequently exerting anti-inflammation and promoting epidermal cell migration and wound healing by secreting IL10, TGFβ and MMP12.

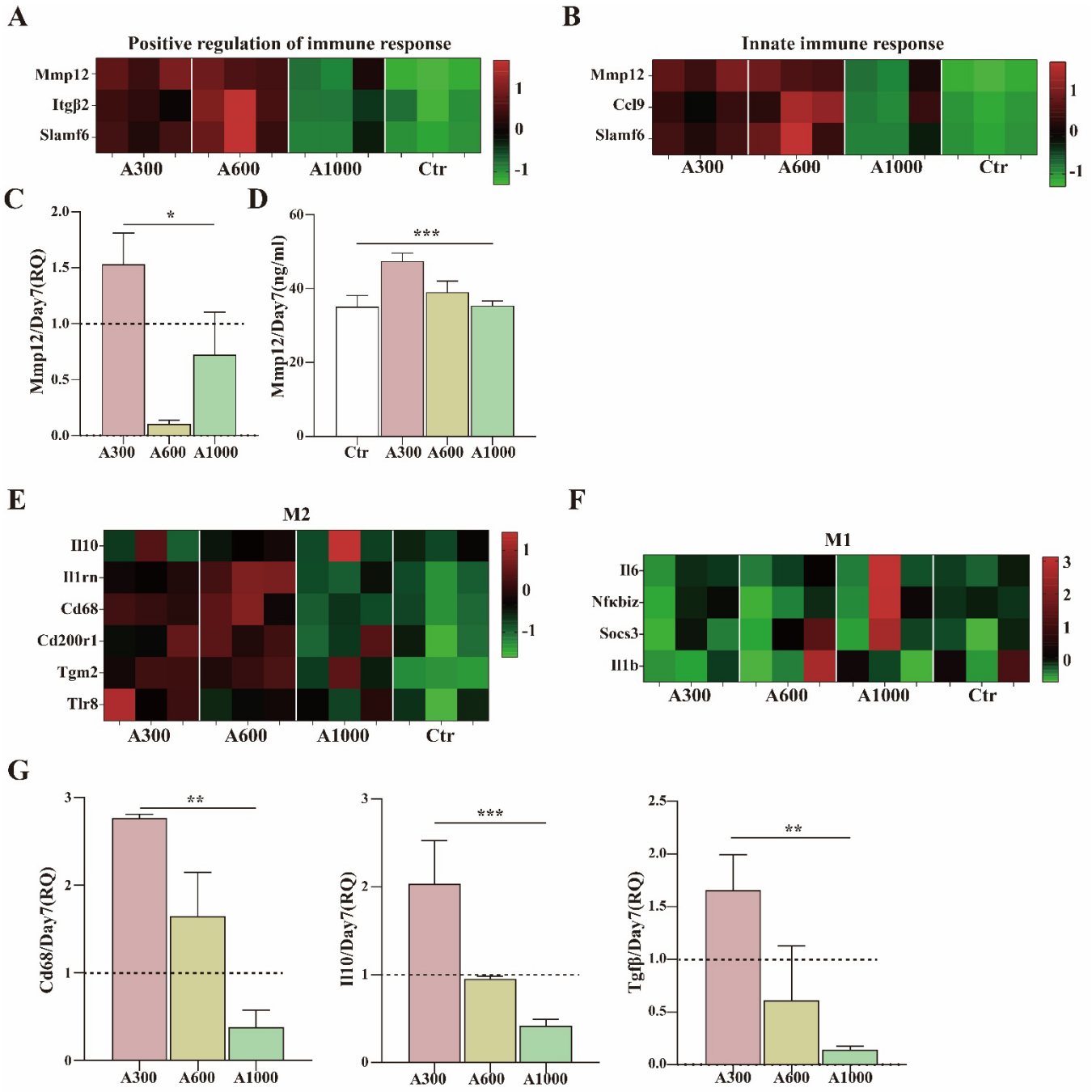

Figure 9. (A) Heat map of *positive regulation of immune response*; (B) Heat map of *innate immune response*; (C) The RNA expression of MMP12; (D) ELISA result of MMP12; (E) Heat map of *M2*; (F) Heat map of *M1*; (G) The RNA expression of Cd68, IL-10 and TGFβ.

4. Conclusions

In the present study, the aligned fish collagen reinforced Poly (lactide-co-glycolide) electrospinning membrane (FC/PLGA) with different diameters were successfully prepared via electrospinning, which has the ability to imitate the skin component and spatial structure of the ECM. The small diameter (A300) significantly enhanced the mechanical strength and hydrophilicity, and accelerated the degradation rate of the fabricated FC/PLGA membrane as desired. The A300 improved the cytocompatibility of the FC/PLGA membrane, such as promoting L929 proliferation and accelerating HOK spread, respectively; in particular, the A300 improved skin wound healing (epithelization and vascularization). More importantly, the transcriptome analysis revealed the underlying molecular mechanism that electrospinning membranes of A300 group could promote macrophages transformation to M2 through phagocytosis, subsequently exerting anti-inflammation and promoting epidermal cell migration and wound healing by secreting IL10, TGFβ and MMP12. Hence, we consider the small diameter aligned electrospinning FC/PLGA fibrous membrane (A300) to be a potential candidate for guided tissue regeneration applications, particularly for the keratinized gingiva.

5. Acknowledgments

This work was supported by ‘National Natural Science Foundation of China’ (No. 81671023 and 81870801).

6. Disclosures

The authors state no conflict of interest.

Supplements

Table S1. Electrospinning parameters of Various Membranes

Diameter Group	Solutions	Voltage	Distance	Speed
Small(A300)	PLGA (20% w/v) FC (2% w/v)		11cm	0.018mm/min
Medium(A600)	PLGA (20% w/v) FC (2% w/v)	-2/5kv	16cm	0.068mm/min
Large(A1000)	PLGA (25% w/v) FC (2% w/v)		16cm	0.068mm/min

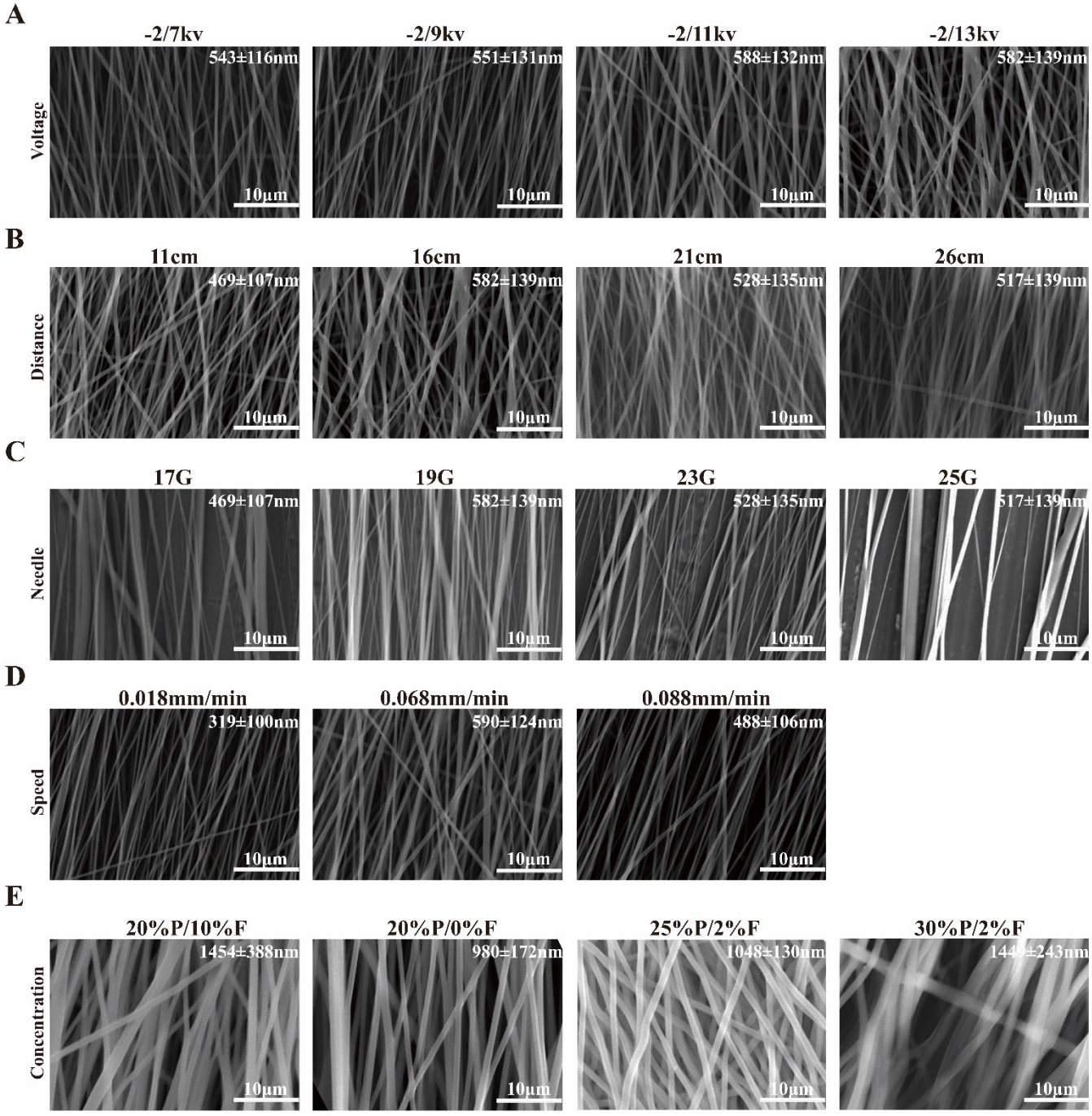

Figure S1. The diameter of the electrospinning fiber could be changed by adjusting (A) the voltage, (B) the distance from the tip to the collector, (C) the inner diameter of the needle, (D) the injection rate and (E) the concentration of the solution. P: PLGA, F: FC.

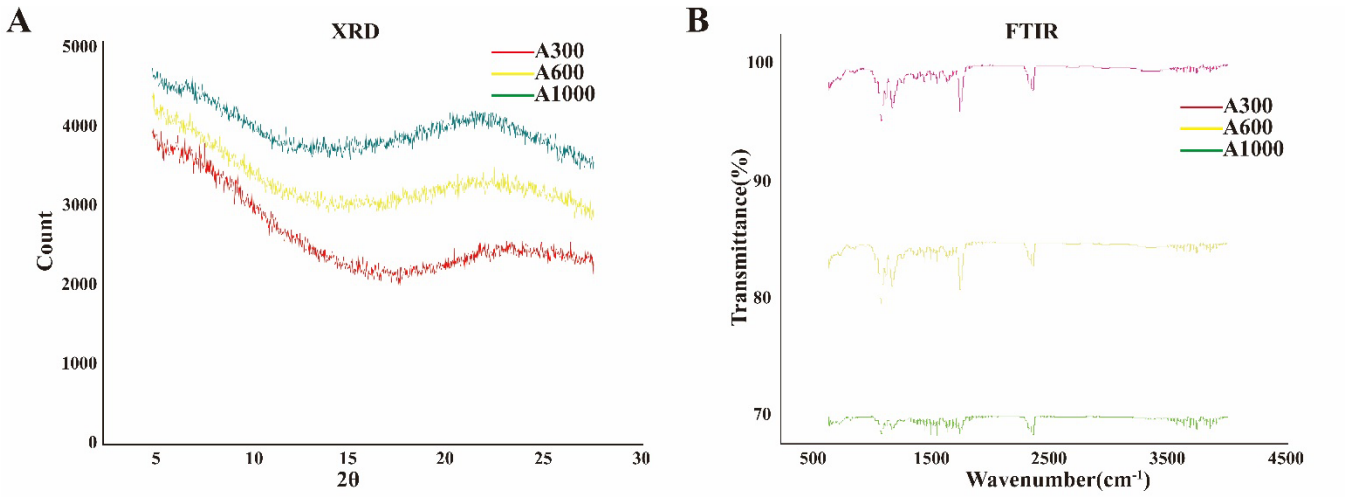

Figure S2. (A) XRD patterns of various membranes; (B) FTIR spectra of various membranes.

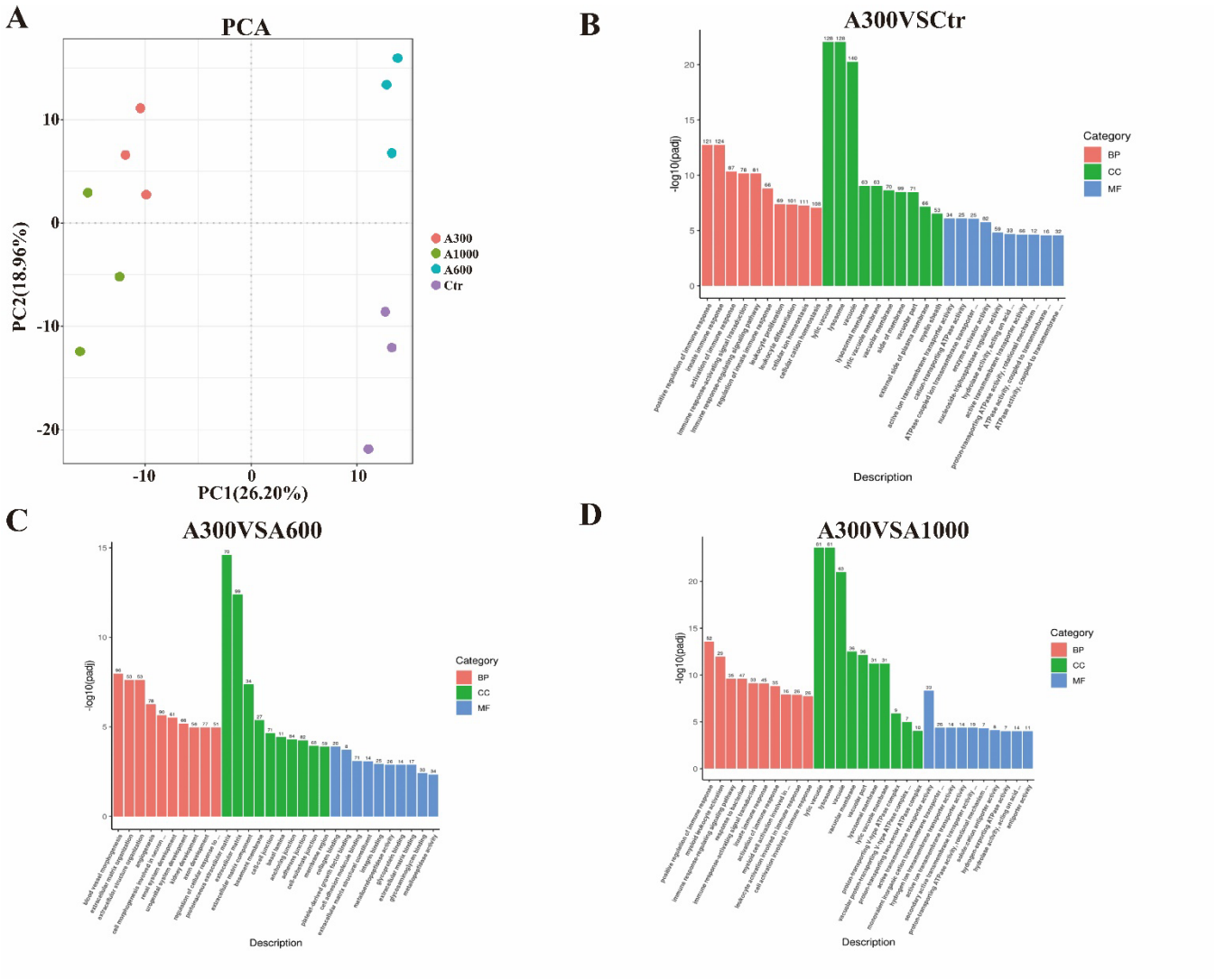

Figure S3. (A) PCA images of Bulk RNA Sequence; (B) A300*VS*Ctr, (C) A300*VS* A600 and (D) A300*VS* A1000 of GO of Bulk RNA Sequence on day 7.

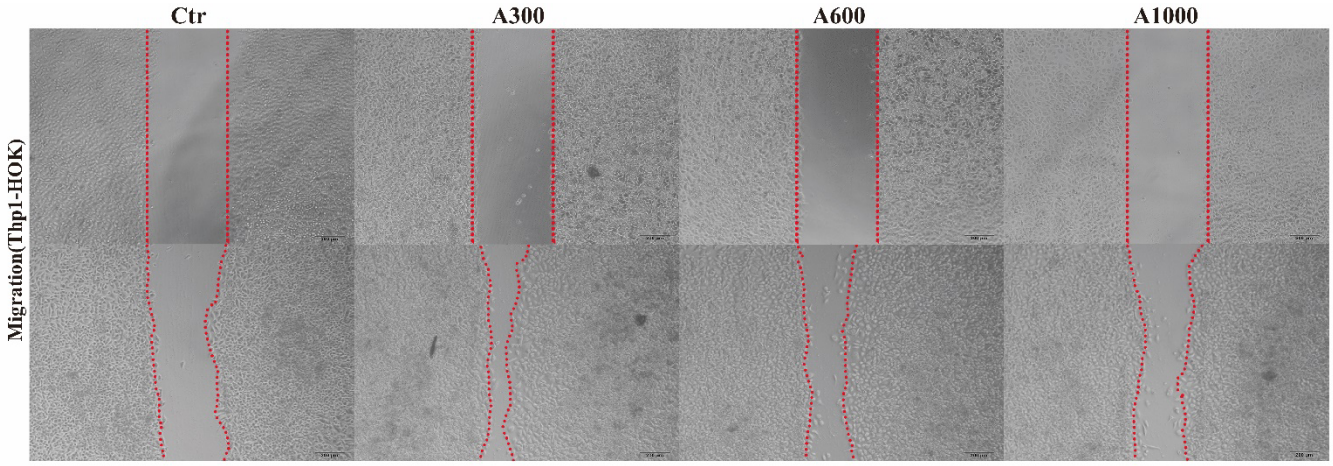

Figure S4. The migration of HOK was stimulated by the conditioned medium derived from Thp1 inoculated on different diameter electrospinning membranes.

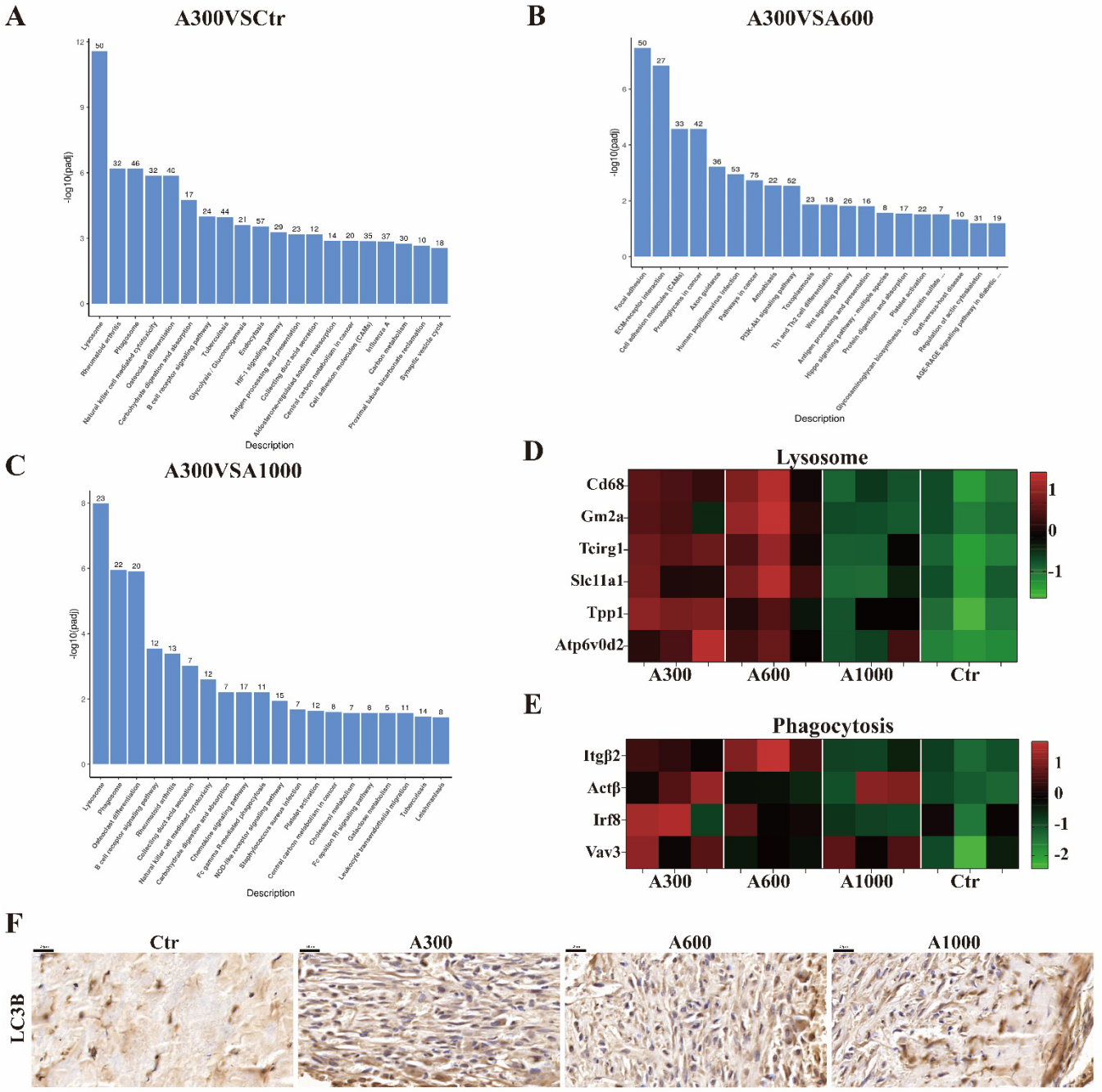

Figure S5. (A) A300VSCtr, (B) A300VS A600 and (C) A300VS A1000 of KEGG of Bulk RNA Sequence on day 7; (D) Heat map of *lysosome*; (E) Heat map of *phagocytosis*; (F) LC3B-positive images of immunohistochemical staining of rat skin defects.

References

[1] Amirsadeghi A, Jafari A, Eggermont L J, et al. Vascularization strategies for skin tissue engineering[J]. Biomater Sci, 2020, 8(15): 4073-4094.

[2] Zhao Y, Li Z, Song S, et al. Skin□Inspired Antibacterial Conductive Hydrogels for Epidermal Sensors and Diabetic Foot Wound Dressings[J]. Advanced Functional Materials, 2019, 29.

[3] Sen C K, Gordillo G M, Roy S, et al. Human skin wounds: a major and snowballing threat to public health and the economy[J]. Wound Repair Regen, 2009, 17(6): 763-71.

[4] Blacklow S O, Li J, Freedman B R, et al. Bioinspired mechanically active adhesive dressings to accelerate wound closure[J]. Sci Adv, 2019, 5(7): eaaw3963.

[5] Savoji H, Godau B, Hassani M S, et al. Skin Tissue Substitutes and Biomaterial Risk Assessment and Testing[J]. Front Bioeng Biotechnol, 2018, 6: 86.

[6] Wang P H, Huang B S, Horng H C, et al. Wound healing[J]. J Chin Med Assoc, 2018, 81(2): 94-101.

[7] Cui L, Liang J, Liu H, et al. Nanomaterials for Angiogenesis in Skin Tissue Engineering[J]. Tissue Eng Part B Rev, 2020, 26(3): 203-216.

[8] Larouche J, Sheoran S, Maruyama K, et al. Immune Regulation of Skin Wound Healing: Mechanisms and Novel Therapeutic Targets[J]. Adv Wound Care (New Rochelle), 2018, 7(7): 209-231.

[9] Friedl P, Wolf K. Plasticity of cell migration: a multiscale tuning model[J]. J Cell Biol, 2010, 188(1): 11-9.

[10] Scadden D T. Nice neighborhood: emerging concepts of the stem cell niche[J]. Cell, 2014, 157(1): 41-50.

[11] Miguel S P, Figueira D R, Simões D, et al. Electrospun polymeric nanofibres as wound dressings: A review[J]. Colloids Surf B Biointerfaces, 2018, 169: 60-71.

[12] Juncos Bombin A D, Dunne N J, Mccarthy H O. Electrospinning of natural polymers for the production of nanofibres for

wound healing applications[J]. Mater Sci Eng C Mater Biol Appl, 2020, 114: 110994.

[13] Kishan A P, Cosgriff-Hernandez E M. Recent advancements in electrospinning design for tissue engineering applications: A review[J]. J Biomed Mater Res A, 2017, 105(10): 2892-2905.

[14] Wang Y, Shi H, Qiao J, et al. Electrospun tubular scaffold with circumferentially aligned nanofibers for regulating smooth muscle cell growth[J]. ACS Appl Mater Interfaces, 2014, 6(4): 2958-62.

[15] Nour S, Imani R, Chaudhry G R, et al. Skin wound healing assisted by angiogenic targeted tissue engineering: A comprehensive review of bioengineered approaches[J]. J Biomed Mater Res A, 2020.

[16] Doyle A D, Carvajal N, Jin A, et al. Local 3D matrix microenvironment regulates cell migration through spatiotemporal dynamics of contractility-dependent adhesions[J]. Nat Commun, 2015, 6: 8720.

[17] Li F, Li B, Wang Q M, et al. Cell shape regulates collagen type I expression in human tendon fibroblasts[J]. Cell Motil Cytoskeleton, 2008, 65(4): 332-41.

[18] Liu Y, Franco A, Huang L, et al. Control of cell migration in two and three dimensions using substrate morphology[J]. Exp Cell Res, 2009, 315(15): 2544-57.

[19] Xie J, Macewan M R, Ray W Z, et al. Radially aligned, electrospun nanofibers as dural substitutes for wound closure and tissue regeneration applications[J]. ACS Nano, 2010, 4(9): 5027-36.

[20] Alford P W, Nesmith A P, Seywerd J N, et al. Vascular smooth muscle contractility depends on cell shape[J]. Integr Biol (Camb), 2011, 3(11): 1063-70.

[21] Abrigo M, Mcarthur S L, Kingshott P. Electrospun nanofibers as dressings for chronic wound care: advances, challenges, and future prospects[J]. Macromol Biosci, 2014, 14(6): 772-92.

[22] Mcbeath R, Pirone D M, Nelson C M, et al. Cell shape, cytoskeletal tension, and RhoA regulate stem cell lineage commitment[J]. Dev Cell, 2004, 6(4): 483-95.

[23] Jafari A, Amirsadeghi A, Hassanajili S, et al. Bioactive antibacterial bilayer PCL/gelatin nanofibrous scaffold promotes full-thickness wound healing[J]. Int J Pharm, 2020, 583: 119413.

[24] Kumbar S G, Nukavarapu S P, James R, et al. Electrospun poly(lactic acid-co-glycolic acid) scaffolds for skin tissue engineering[J]. Biomaterials, 2008, 29(30): 4100-7.

[25] Liu Y, Ji Y, Ghosh K, et al. Effects of fiber orientation and diameter on the behavior of human dermal fibroblasts on electrospun PMMA scaffolds[J]. J Biomed Mater Res A, 2009, 90(4): 1092-106.

[26] Hodgkinson T, Yuan X F, Bayat A. Electrospun silk fibroin fiber diameter influences in vitro dermal fibroblast behavior and promotes healing of ex vivo wound models[J]. J Tissue Eng, 2014, 5: 2041731414551661.

[27] Saino E, Focarete M L, Gualandi C, et al. Effect of electrospun fiber diameter and alignment on macrophage activation and secretion of proinflammatory cytokines and chemokines[J]. Biomacromolecules, 2011, 12(5): 1900-11.

[28] Chen H, Qian Y, Xia Y, et al. Enhanced Osteogenesis of ADSCs by the Synergistic Effect of Aligned Fibers Containing Collagen I[J]. ACS Appl Mater Interfaces, 2016, 8(43): 29289-29297.

[29] Jin S, Sun F, Zou Q, et al. Fish Collagen and Hydroxyapatite Reinforced Poly(lactide-co-glycolide) Fibrous Membrane for Guided Bone Regeneration[J]. Biomacromolecules, 2019, 20(5): 2058-2067.

[30] Liu S-D, Li D-S, Yang Y, et al. Fabrication, mechanical properties and failure mechanism of random and aligned nanofiber membrane with different parameters[J]. Nanotechnology Reviews, 2019, 8: 218-226.

[31] Da Cunha M R, Menezes F A, Dos Santos G R, et al. Hydroxyapatite and a New Fibrin Sealant Derived from Snake Venom as Scaffold to Treatment of Cranial Defects in Rats[J]. Materials Research-Ibero-American Journal of Materials, 2015, 18(1): 196-203.

[32] Gittens R A, Olivares-Navarrete R, Mclachlan T, et al. Differential responses of osteoblast lineage cells to nanotopographically-modified, microroughened titanium-aluminum-vanadium alloy surfaces[J]. Biomaterials, 2012, 33(35):

8986-94.

[33] Chen Z, Bachhuka A, Han S, et al. Tuning Chemistry and Topography of Nanoengineered Surfaces to Manipulate Immune Response for Bone Regeneration Applications[J]. ACS Nano, 2017, 11(5): 4494-4506.

[34] Mulholland E J. Electrospun Biomaterials in the Treatment and Prevention of Scars in Skin Wound Healing[J]. Front Bioeng Biotechnol, 2020, 8: 481.

[35] Stachewicz U, Bailey R, Wang W, et al. Size dependent mechanical properties of electrospun polymer fibers from a composite structure[J]. Polymer, 2012, 53: 5132.

[36] Tan E P, Ng S Y, Lim C T. Tensile testing of a single ultrafine polymeric fiber[J]. Biomaterials, 2005, 26(13): 1453-6.

[37] Giljean S, Bigerelle M, Anselme K. Roughness statistical influence on cell adhesion using profilometry and multiscale analysis[J]. Scanning, 2014, 36(1): 2-10.

[38] Miguel S P, Sequeira R S, Moreira A F, et al. An overview of electrospun membranes loaded with bioactive molecules for improving the wound healing process[J]. Eur J Pharm Biopharm, 2019, 139: 1-22.

[39] Zhong S, Teo W E, Zhu X, et al. An aligned nanofibrous collagen scaffold by electrospinning and its effects on in vitro fibroblast culture[J]. J Biomed Mater Res A, 2006, 79(3): 456-63.

[40] Chomachayi M D, Solouk A, Mirzadeh H. Electrospun silk-based nanofibrous scaffolds: fiber diameter and oxygen transfer[J]. Prog Biomater, 2016, 5: 71-80.

[41] Tian F, Hosseinkhani H, Hosseinkhani M, et al. Quantitative analysis of cell adhesion on aligned micro- and nanofibers[J]. J Biomed Mater Res A, 2008, 84(2): 291-9.

[42] Lavenus S, Pilet P, Guicheux J, et al. Behaviour of mesenchymal stem cells, fibroblasts and osteoblasts on smooth surfaces[J]. Acta Biomater, 2011, 7(4): 1525-34.

[43] Baker B M, Trappmann B, Wang W Y, et al. Cell-mediated fibre recruitment drives extracellular matrix mechanosensing

in engineered fibrillar microenvironments[J]. Nat Mater, 2015, 14(12): 1262-8.

[44] Babakhani A, Nobakht M, Pazoki Torodi H, et al. Effects of Hair Follicle Stem Cells on Partial-Thickness Burn Wound Healing and Tensile Strength[J]. Iran Biomed J, 2020, 24(2): 99-109.

[45] Chen F, Zhang Q, Wu P, et al. Green fabrication of seedbed-like Flammulina velutipes polysaccharides-derived scaffolds accelerating full-thickness skin wound healing accompanied by hair follicle regeneration[J]. Int J Biol Macromol, 2021, 167: 117-129.

[46] Sahana T G, Rekha P D. Biopolymers: Applications in wound healing and skin tissue engineering[J]. Mol Biol Rep, 2018, 45(6): 2857-2867.

[47] Franz S, Rammelt S, Scharnweber D, et al. Immune responses to implants - a review of the implications for the design of immunomodulatory biomaterials[J]. Biomaterials, 2011, 32(28): 6692-709.

[48] Anderson J M, Rodriguez A, Chang D T. Foreign body reaction to biomaterials[J]. Semin Immunol, 2008, 20(2): 86-100.

[49] Chu C, Liu L, Rung S, et al. Modulation of foreign body reaction and macrophage phenotypes concerning microenvironment[J]. J Biomed Mater Res A, 2019.

[50] Bryers J D, Giachelli C M, Ratner B D. Engineering biomaterials to integrate and heal: the biocompatibility paradigm shifts[J]. Biotechnol Bioeng, 2012, 109(8): 1898-911.

[51] Wolf M, Maltseva I, Clay S M, et al. Effects of MMP12 on cell motility and inflammation during corneal epithelial repair[J]. Exp Eye Res, 2017, 160: 11-20.

[52] Chan M F, Li J, Bertrand A, et al. Protective effects of matrix metalloproteinase-12 following corneal injury[J]. J Cell Sci, 2013, 126(Pt 17): 3948-60.

[53] Shapiro S D, Kobayashi D K, Ley T J. Cloning and characterization of a unique elastolytic metalloproteinase produced by human alveolar macrophages[J]. J Biol Chem, 1993, 268(32): 23824-9.

[54] Huang S M, Wu C S, Chiu M H, et al. High glucose environment induces M1 macrophage polarization that impairs keratinocyte migration via TNF-α: An important mechanism to delay the diabetic wound healing[J]. J Dermatol Sci, 2019, 96(3): 159-167.

[55] Usui M L, Mansbridge J N, Carter W G, et al. Keratinocyte migration, proliferation, and differentiation in chronic ulcers from patients with diabetes and normal wounds[J]. J Histochem Cytochem, 2008, 56(7): 687-96.

[56] Daley J M, Brancato S K, Thomay A A, et al. The phenotype of murine wound macrophages[J]. J Leukoc Biol, 2010, 87(1): 59-67.

[57] Elliott M R, Koster K M, Murphy P S. Efferocytosis Signaling in the Regulation of Macrophage Inflammatory Responses[J]. J Immunol, 2017, 198(4): 1387-1394.